Picosecond dissociation of amyloid fibrils with infrared laser: A nonequilibrium simulation study

Man Hoang Viet, Philippe Derreumaux, Mai Suan Li, Christopher Roland, Celeste Sagui, and Phuong H. Nguyen

Citation: The Journal of Chemical Physics **143**, 155101 (2015); doi: 10.1063/1.4933207
View online: http://dx.doi.org/10.1063/1.4933207
View Table of Contents: http://scitation.aip.org/content/aip/journal/jcp/143/15?ver=pdfcov
Published by the AIP Publishing

Picosecond dissociation of amyloid fibrils with infrared laser: A nonequilibrium simulation study

Man Hoang Viet,[1] Philippe Derreumaux,[2] Mai Suan Li,[3,4] Christopher Roland,[1,a)] Celeste Sagui,[1,b)] and Phuong H. Nguyen[2,c)]
[1]*Department of Physics, North Carolina State University, Raleigh, North Carolina 27695-8202, USA*
[2]*Laboratoire de Biochimie Théorique, UPR 9080, CNRS Université Denis Diderot, Sorbonne Paris Cité IBPC, 13 rue Pierre et Marie Curie, 75005 Paris, France*
[3]*Institute of Physics, Polish Academy of Sciences, Al. Lotnikow 32/46, 02-668 Warsaw, Poland*
[4]*Institute for Computational Science and Technology, SBI Building, Quang Trung Software City, Tan Chanh Hiep Ward, District 12, Ho Chi Minh City, Vietnam*

(Received 23 July 2015; accepted 2 October 2015; published online 20 October 2015)

Recently, mid-infrared free-electron laser technology has been developed to dissociate amyloid fibrils. Here, we present a theoretical framework for this type of experiment based on laser-induced nonequilibrium all-atom molecular dynamics simulations. We show that the fibril is destroyed due to the strong resonance between its amide I vibrational modes and the laser field. The effects of laser irradiation are determined by a balance between fibril formation and dissociation. While the overall rearrangements of the fibril finish over short time scales, the interaction between the peptides and the solvent continues over much longer times indicating that the waters play an important role in the dissociation process. Our results thus provide new insights into amyloid fibril dissociation by laser techniques and open up new venues to investigate the complex phenomena associated with amyloidogenesis. © *2015 AIP Publishing LLC.* [http://dx.doi.org/10.1063/1.4933207]

I. INTRODUCTION

A number of proteins and peptides have been found to aggregate into insoluble amyloid fibrils composed of cross β-sheets stabilized by backbone hydrogen bonds (HBs).[1,2] In human brains, fibrils are associated with several neurodegenerative diseases, such as Alzheimer's and Parkinson's disease.[3,4] Experimentally, amyloid fibrils can be detected and removed with chemicals such as guanidine hydrochloride or dimethyl sulfoxide.[5] Since these chemicals are highly toxic and harmful, alternative methods for their removal are being sought. For example, the ultrasound technique has been developed to disrupt and remove amyloid fibrils.[6,7] Recently, new laser technology has been developed and applied to the amyloid field.[8–14] In particular, Kawasaki and coworkers have developed a mid-infrared free-electron laser (FEL) having specific oscillation characteristics of a picosecond pulse structure, a tunable wavelength within infrared frequencies, and a high photon density. Tuning the laser frequency to the amide I bands, they were able to dissociate amyloid-like fibrils of lysozyme into their native forms,[11] convert insulin fibrils into soluble monomers,[12] and dissociate a fibril of a short peptide from human thyroid hormone.[13,14] However, it is unclear from these experiments whether the primary step in the dissociation is locally induced by energy deposition into the amide carbonyl bonds or by heating of all degrees of freedom of the fibrils. In addition, the microscopics of the dissociation process is still largely unknown. Moreover, the potential for unwanted photo-damage to the surrounding biological structures remains to be determined. This is especially important if one wants to translate the laser-induced fibril dissociation method into real world applications such as treatment amyloid related diseases.

As a first step in elucidating these issues, we have carried out a comprehensive investigation based on laser-induced nonequilibrium molecular dynamics (NEMD) simulations of a number of select amyloid-based molecules having different architectures in the presence of globular proteins and DNA. We find that amyloid fibrils are destroyed due to the strong resonance between the laser field and the amide I vibrational modes of the fibrils, and surrounding molecules are hardly affected.

II. METHODOLOGY

A. Systems

To demonstrate the robustness of the method, we consider four systems having different architectures: (i) two complexes named as Aβ-PrP-DNA and Aβ-ACP-DNA, where Aβ is a 5-mer cross-β sheet fibril formed by the Alzheimer's disease Aβ_{17-42} peptide,[15] PrP is a 104-residue Prion protein (PrP), ACP is a 98-residue acylphosphatase protein from bovine testis, and DNA is a 24-nucleotide duplex B-DNA. The PrP was chosen because it has been suggested that binding between Aβ and the PrP is necessary for synaptic perturbations.[16] The ACP consists of two parallel and two antiparallel β-sheets, two helix segments thus representing common structures of proteins.[17] These complexes allow us to study the side effects of the laser excitation on surrounding molecules. (ii) The 32-mer double β-sheet fibril formed by the 7-residue peptide segment(GNNQQNY) from Sup35.[18] (iii) The 5-mer

a)Email: cmroland@ncsu.edu
b)Email: sagui@ncsu.edu
c)Email: phuong.nguyen@ibpc.fr

left-handed β solenoid fibril formed by the 79-residue HET-s protein from the filamentous fungus *Podospora anserina*.[19]

The initial structure of the 24-nucleotide B-DNA (sequence: $(5'\text{-CGCGCGCGCGCG-}3')_2$) was taken from the previous work.[20] The initial structures of three fibrils and two proteins were taken from the protein data bank with the Protein Data Bank (PDB) codes: Aβ fibril: 2BEG, Sup35 fibril: 1YJP, HET-s fibril: 2RNM, ACP protein: 2ACY, and PrP: 1QLX. For each complex, we generate 50 initial structures in which the Aβ fibril is free, and 50 initial structures in which the Aβ fibril makes at least one contact with DNA and ACP or PrP. This type of initial structures allows us to study the indirect effect induced by the energy transfer from the hot excited Aβ fibril to surrounding. The initial structures of the systems are shown in Fig. 1.

B. Equilibrium molecular dynamics simulation

For all systems, we use the AMBER-f99SB-ILDN force field (FF)[21] to model the proteins, DNA, and TIP3P water model to describe the solvent. The structures were centered in truncated octahedron simulation boxes filed with 31 609-40 672 waters for the complexes (box-size varies from 10.0 nm to 11.8 nm), 12 224 waters for the Sup35 (box-size: 8.1 nm), and 20 643 waters for the HET-s (box-size: 9.6 nm). The pH is set to 7 with the N-terminus treated as NH_3^+ and the C-terminus as CO_2^-, Arg and Lys positively charged (NH_3^+), Glu and Asp negatively charged (CO_2^-), and the His residues neutral with a hydrogen on the epsilon nitrogen. Finally, the systems are neutralized by adding Na^+ cations. Starting from these structures, short simulations of 1 ns were carried out in NPT ensemble followed by the other 1 ns NVT simulations. Then, 100 independent conformations were selected statistically from the NVT trajectory of each system and subsequently used for the NEMD simulations.

The GROMACS program[22] is used to perform the simulations. The bond lengths with hydrogen atoms are fixed with the SHAKE algorithm[23] and the equations of motion are integrated with a time step of 2 fs using a leapfrog algorithm. The electrostatic interactions are calculated using the particle mesh Ewald method and a cutoff of 1.1 nm.[24] A cutoff of 1.2 nm is used for the van der Waals interactions. The nonbonded pair lists are updated every 10 fs. Temperatures are controlled by the Berendsen thermostat.[25]

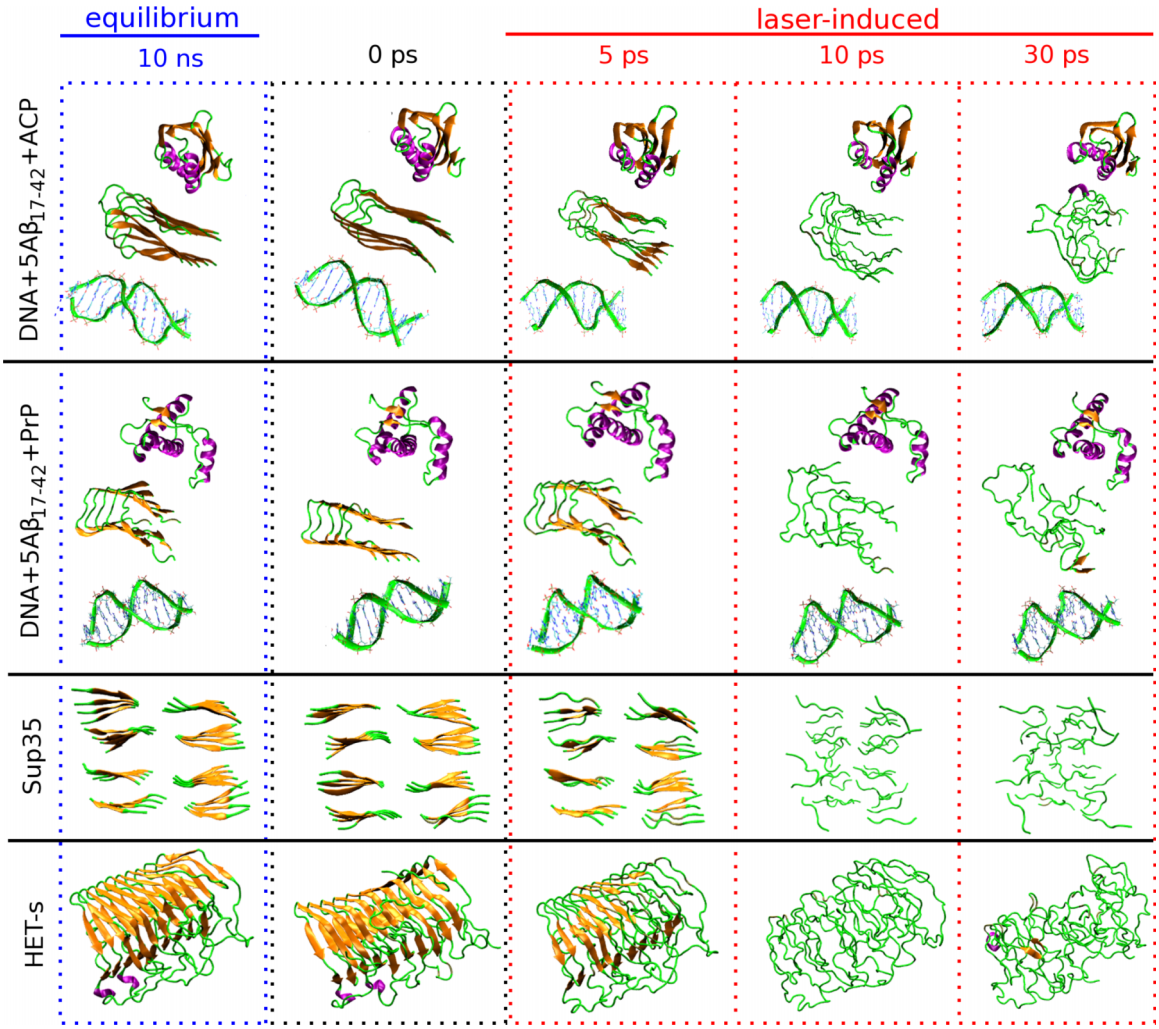

FIG. 1. (0 ps) Initial structures of four systems. The 1st and 2nd rows show the structures of the complexes where the Aβ fibril is in the middle, the ACP proteins, PrPs, and DNA are above and below, respectively. (Left panels) Snapshots at 10 ns of the equilibrium MD simulations. (Right panels) Snapshots at 5, 10, and 30 ps of the laser-induced NEMD simulations using $E_0 = 2$ V nm^{-1}, $\omega = 1671$ cm^{-1}.

C. Laser-induced nonequilibrium molecular dynamics simulation

In a laser-induced NEMD simulation, a time-dependent electric field

$$E(t) = E_0 \exp[-\frac{(t-t_0)^2}{2\sigma^2}] \cos[2\pi c\omega(t-t_0)] \quad (1)$$

was applied to mimic a laser pulse.[26,27] Here, E_0 represents the amplitude of the electric field, σ is the pulse width, t is the time after the pulse maximum t_0, c is the speed of light, and ω is the frequency. This technique has been implemented in the GROMACS simulation package.[22] In a conventional MD simulation, the temperature of the system is typically maintained by rescaling the velocities of all atoms at every time step.[25] In a laser-induced nonequilibrium experiment, the photoexcitation results in a vibrationally hot molecule, which is then cooled via the transfer of the vibrational energy to the surrounding solvent molecules.[28] Thus, in our NEMD simulations, only the waters are coupled to the heat bath in order to maintain the temperature of 310 K with a coupling constant of 0.1 ps. This technique has been developed in previous photo-induced NEMD simulations of peptides[28–33] and validated by comparing the cooling times with known experimental results.[28,31] This also mimics the experiment conditions, in which water is added periodically to the suspension during the irradiation process in order to prevent excessive evaporating.[11–14] To ensure stability, a time step of 0.2 fs was used, and data were collected every 0.1 ps.

D. Data analysis

The secondary structures of proteins are calculated using STRIDE.[34] The eight STRIDE structures were grouped into four structures: β = extended + bridge, α = α-helix + 3_{10}-helix, turn = turn + bend, and coil = coil + PII-helix. Note that the percentage of 3_{10}- and PII-helices is very low in the present simulations.

A contact is defined if the distance between two heavy-atoms is less than 0.45 nm. A hydrogen bond (H-bond) was considered formed when the acceptor-donor distance is not more than 0.35 nm and the acceptor-donor-hydrogen angle is not more than 30°.

The vibrational IR spectrum is calculated only for the initial structure in the gas phase using the normal mode harmonic approximation. The intensities are obtained from derivatives of the dipole moment and the polarizability along the vibrational normal modes. By this means, the integral IR absorption coefficient of normal mode p is given by[35]

$$A = \frac{1}{4\pi\epsilon_0}\frac{N_A\pi}{3c^2}\left(\frac{\partial\mu}{\partial Q_p}\right), \quad (2)$$

where Q_p denotes the mass-weighted normal coordinate corresponding to normal mode p, N_A is Avogadro's constant, c is the speed of light, and ϵ_0 is the vacuum permittivity. The derivative of the dipole moment has to be evaluated at the equilibrium structure. All calculations are done using the GROMACS simulation package.[22]

III. RESULTS AND DISCUSSION

In the following, we present results of four systems described above. First, we present the static vibrational IR spectra and identify the amide I vibrational modes of the fibril structures. Then, we scan the laser frequency to obtain the resonance with the fibrils. Adopting the Aβ-ACP-DNA complex as a representative example, we investigate the laser-induced dissociation resonant mechanisms in details. The robustness of the laser-excitation method is then demonstrated with the other systems.

A. Vibrational IR spectrum

As we aim to excite the amide I modes, we first calculate the vibrational IR spectrum [Eq. (2)], then identify the amide I band frequency and absorption intensity for each system. Because it is known that the usual biophysical FFs such as AMBER,[21] CHARMM,[36] OPLS,[37] and GROMOS[38] were not aimed to produce accurately high frequency motions such as amide I modes; thus, an issue that deserves some attention is the question of whether the results depend on the FFs. To this end, we calculated the IR spectra of the Aβ fibril and PrP, ACP proteins employing four FFs mentioned above. For the Aβ fibril, Fig. 2(a) shows that the AMBER and CHARMM FFs exhibit dominant peaks of the amide I bands at 1671 and 1675 cm^{-1}, respectively. In contrast, the OPLS and GROMOS FFs do not show clearly the absorption intensities [Fig. 2(d)]. For the PrP, it is rich in α-helix structure; thus, its amide I band is located at higher frequencies around, respectively, 1687 and 1692 cm^{-1} obtained using AMBER and CHARMM FFs [Fig. 2(b)]. The ACP is dominated by the β-sheet structure; thus, its amide I band is shifted to lower frequencies around 1669 and 1674 cm^{-1} calculated using AMBER and CHARMM FFs [Fig. 2(c)]. Both OPLS and GROMOS FFs do not show clearly the amide I peaks of the PrP and ACP proteins [Figs. 2(e) and 2(f)]. From these results, in this work, we decided to use the AMBER FF for all subsequent calculations. With this FF, the IR spectra of the Sup35 and HET-s fibrils, shown in Fig. 3(b), display the absorption amide I bands around 1671 cm^{-1}, reflecting the vibration of the parallel β-sheet architectures. A closer inspection reveals that the spectrum of the Sup35 fibril also contains two additional peaks around 1655 and 1713 cm^{-1}, which are associated with the vibrations of the antiparallel β-sheet structure. We note that three fibrils exhibit different absorption intensities due to the fact that they are different in architectures and in the numbers of the C=O groups participating in the amide I bands (125 C=O bonds in Aβ, 192 C=O bonds in Sup35, and 395 C=O bonds in HET-s).

B. Resonance between fibril amide I vibrations and laser field

In the experiments of Kawasaki *et al.*, the authors used macro-pulses having duration of 2 μs, each consists of 2-ps micro-pulses separated by an interval of 350 ps. This means each macro-pulse contains about 6000 micro-pulses. The energy of a laser micro-pulse is in the range of 6-8 mJ.

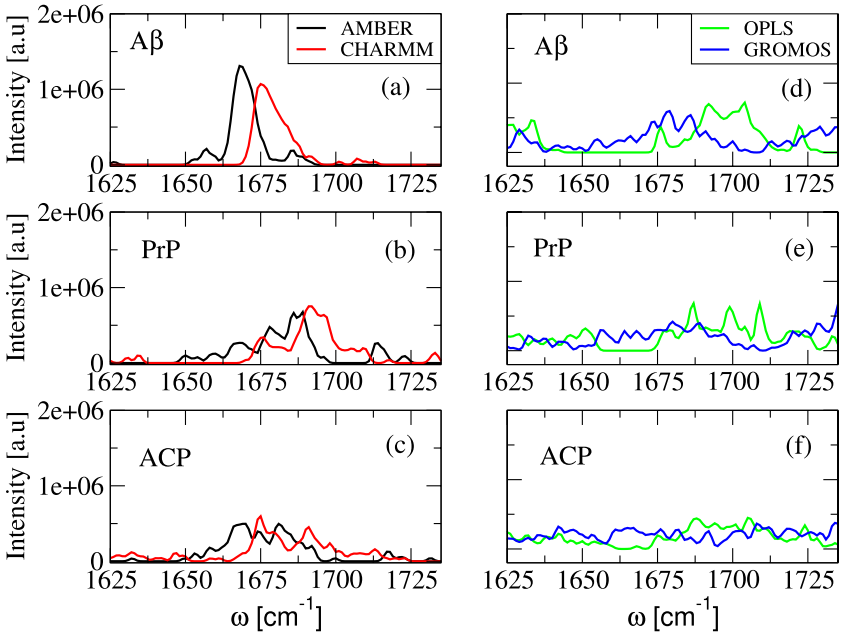

FIG. 2. The vibrational IR spectra of the Aβ fibril (a) and (d), PrP protein (b) and (e), and ACP protein (c) and (f) calculated using various force fields AMBER-f99SB-ILDN (black), CHARMM22 (red), OPLS (green), and GROMOS43a1 (blue).

The fibrils are irradiated for several hours.[11–14] In our simulations, we include the electric field, [Eq. (1)], to mimic the experimental laser. Physically, our toy-laser-model allows us to capture the essential features of experimentally used pulses such as frequency, pulse width, and the magnitude of the field. In principle, we can mimic the experimental conditions by using multiple pulses with time interval of 350 ps but then the NEMD simulations must be run much longer. Given that the large system-sizes and multiple trajectories are required, the simulations are too expensive with current computer resources. However, as the main aim of this work is to show, as a proof of concept, that fibrils can be destroyed due to the resonance between the laser and the amide I vibrational modes, the toy-laser-model we used here is sufficient. With this in mind, we set the pulse width $\sigma = 2$ ps, $t_0 = 5$ ps as used in experiments but varied the strength E_0 so that the fibrils dissociate within a reasonable time scale. The electric field, [Eq. (1)], is shown in Fig. 3(a).

To obtain the resonant laser frequency, for each system, we carried out 2650 NEMD simulations: 10 trajectories, each lasting 16 ps, starting from the conformations selected from a 1 ns equilibrium MD trajectory at 310 K; each trajectory was run with 5 values of E_0 from 0 to 4 V nm^{-1} and 53 values of ω from 1630 to 1730 cm^{-1}. For each (E_0,ω) set, we calculated last values (at 16 ps) of the fibril hydrogen bonds (fibril HBs), root-mean-squared deviation (RMSD) with

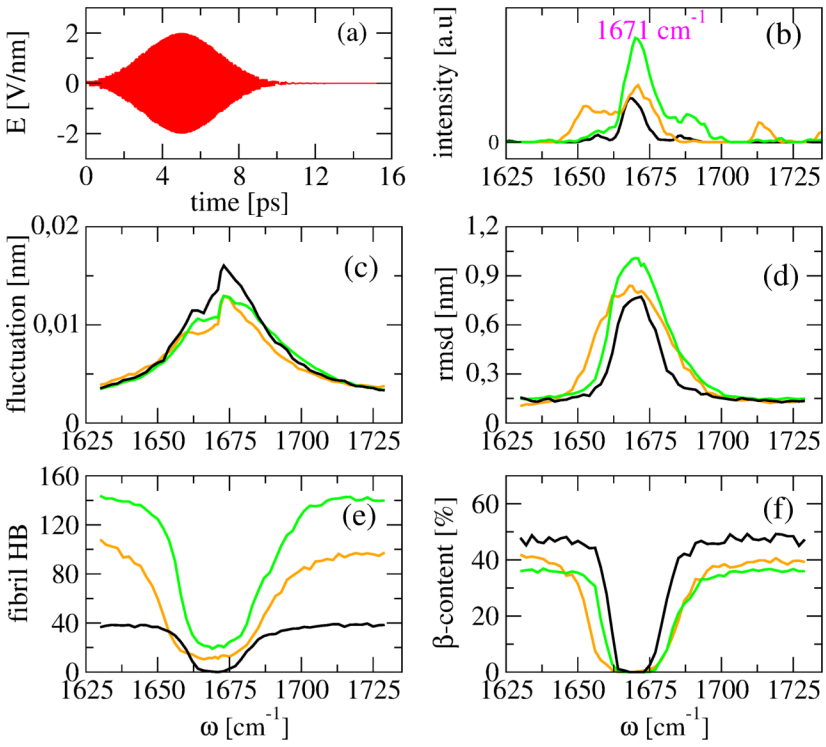

FIG. 3. (a) Time evolution of the electric field with $\omega = 1671$ cm^{-1}, (b) vibrational IR spectra of the initial structure of fibrils, (c) laser-induced changes of the C=O amide I bond lengths, (d) RMSD with respect to fibril structure, (e) the number of fibril hydrogen bonds, and (f) the β structure content. Results are shown with the laser amplitude $E_0 = 2$ V nm^{-1} for the Aβ of the Aβ-ACP-DNA complex (black), Sup35 (orange), and HET-s (green) systems.

respect to the initial structure, the β-content, and results are averaged over all trajectories. We also calculated the maximal values of the C═O bond length fluctuations, which are determined as follows. First, we calculated the fluctuation: $\Delta_i(t) = |d_i(t) - 0.123|$, where $d_i(t)$ is the time evolution of the ith C═O bond length and 0.123 nm is its equilibrium value. Then, we calculated the ensemble average $\langle\Delta(t)\rangle$ by averaging over all trajectories and all C═O bonds in the fibrils (125 C═O bonds in Aβ, 192 C═O bonds in Sup35, and 395 C═O bonds in HET-s). We then determine the maximal value of $\langle\Delta(t)\rangle$. To illustrate the system response to the field, Fig. 3 shows these quantities for a representative case with $E_0 = 2$ V nm^{-1}. As seen, all three systems exhibit a strong resonance with the field at $\omega = 1671 \pm 2$ cm^{-1}, which represents the peaks of the amide I spectra of the initial fibril structures [Fig. 3(b)], as indicated by large changes in the C═O bond lengths and the RMSD [Figs. 3(c) and 3(d)]. The fibril HB number and the β-sheet content are almost zero [Figs. 3(e) and 3(f)]. This indicates that the laser excited primarily the amide I modes of the fibril, supporting the experimental results,[11–14] and that these are enough to dissociate the fibrils as clearly seen from snapshots of the configurations are shown in Fig. 1. Note that although the IR spectrum of the Sup35 fibril exhibits three absorption peaks [Fig. 3(b)], only the excitation at $\omega = 1671$ cm^{-1} results in the dissociation. This is because (i) the intensity at $\omega = 1671$ cm^{-1} is stronger than that of the other two peaks, and (ii) this frequency is associated with the vibration of the C═O groups which form HBs between parallel β-strands. Since the fibril is stabilized by this HB network, the resonance at $\omega = 1671$ cm^{-1} results easily in the dissociation of the whole fibril. In contrast, the frequencies 1655 and 1713 cm^{-1} are associated with the vibrations of the C═O groups which form HBs between antiparallel β-sheets. Since this HB network is not responsible for the fibril stabilization, the resonance at these two frequencies does not destroy the fibril. It is also of interest to note that although the Aβ fibril has the smallest IR absorption intensity, its conformational responses are comparable with those of the Sup35 and HET-s fibrils. This is because, in general, the conformational changes depend not only on the HB network but also on the other interactions. It could happen that a fibril exhibits a strong absorption intensity of the C═O groups, but if its structure is strongly stabilized by the hydrophobic interaction between residues, then the excitation of the amide I modes will not result in large conformational responses.

C. Laser-induced dissociation of the Aβ-ACP-DNA complex

Having identified resonant frequency, we wish to study the laser-induced dissociation mechanisms in details, considering the Aβ-ACP-DNA complex as a representative example. To this end, we carried out 100 NEMD simulations starting from the equilibrium selected structures, each lasting 50 ps using $\omega = 1671$ cm^{-1} and $E_0 = 2$ V nm^{-1}. Fig. 4(a) shows the time-evolution of the C═O bond length fluctuation averaged over 125 C═O bonds and 100 trajectories. As seen, the C═O atoms absorb energy after 2 ps, and the bond length increases from the equilibrium value to the maximal value of ~0.0135 nm after 3.5 ps. The excess C═O stretching potential energy is then converted to the kinetic energy and heats locally the C═O atoms. Indeed, Fig. 4(b) shows, as a representative example, the kinetic energy of the backbone, side-chain atoms of the Met35 residue of the Aβ fibril. This residue is selected because its long side-chain [Fig. 4(b), inset] allows for a demonstration of energy transfer process. As seen, the kinetic energies of the C, O atoms increase and reach the maximal values a bit later, around 4 ps. Then, the pulse intensity decreases leading to the decay in the C═O bond lengths and kinetic energy [Figs. 4(a) and 4(b)]. During this time, energy absorbed by the

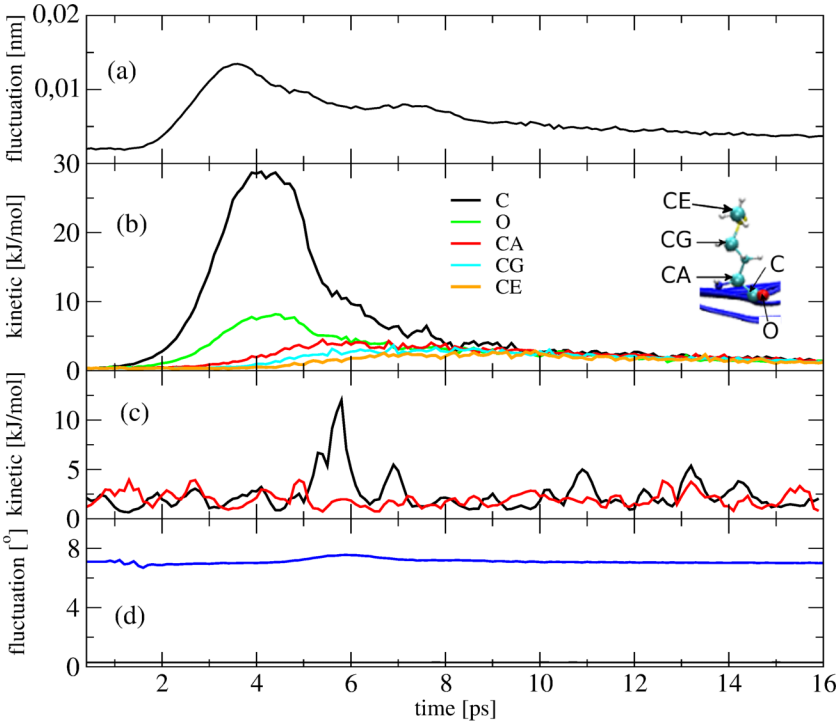

FIG. 4. Time evolution of (a) the fluctuation of the C═O amide I bond lengths, (b) the kinetic energy of various atoms of the MET35 residue (inset picture), (c) the kinetic energy of the waters in the first solvation shell (black) and far from the fibril (red), and (d) the fluctuation of the HOH angle-bending of the rigid (black) and flexible TIP3P waters (blue). Shown are results obtained using $\omega = 1671$ cm^{-1}, $E_0 = 2$ V nm^{-1}.

amide I modes is rapidly redistributed to other intramolecular vibrational modes and also to water molecules. For example, the C_α and side-chain atoms of the MET35 residue receive energy after ~4 ps and their kinetic energies reach the maximal values at latter time ~6 ps [Fig. 4(b)]. Interestingly, the CE atom, which is far from the hot C═O group, receives less energy, indicating that energy transfers primarily via covalent bonds. Since the temperature of the waters is maintained at 310 K via the continuous rescaling of the velocities, the cooling process is very efficient. Indeed, as shown in Fig. 4(c), only waters in the first solvation shell receive some kinetic energies at ~6 ps, which then quickly decay to equilibrium values. The bulk waters are hardly heated. We should mention that in experiments, water is added periodically to the suspension during irradiation to avoid water evaporation, and temperature increases only 2°–3°.[11–14] In this context, our simulation technique correctly mimics the experiments. After 10 ps, the pulse has vanished and the system has cooled down. The system reaches its equilibrium state at around 30 ps.

An issue that deserves some attention is the question of whether the results depend on water models. In this work, we use the rigid TIP3P water model. As shown, the physics behind the dissociation is the resonance between the field and amide I vibrational modes of the fibril. It is known that the water-bending vibrational mode is nearly resonant with the amide I vibration; therefore, it is possible that waters are also excited due to the energy transferred from the amide I modes and absorbed from the laser. To clarify, we carried out additional NEMD simulations for the Aβ-ACP-DNA system using the TIP3P flexible water model.[39] Fig. 4(d) shows the fluctuation of the HOH angle-bending of waters in the first solvation shell around the Aβ fibril. As expected, the rigid waters do not undergo any angle-bending vibration. The flexible waters exhibit the angle fluctuation ~7° around equilibrium value. Larger fluctuations ~7.5° are observed at ~6 ps and coincide with the maximal value of kinetic energy [Fig. 4(c)]. We also find that the fibril dissociation process is hardly affected by the use of the flexible waters (data not shown). This is not surprising because in the simulations, waters are coupled to the heat bath and their excess energy is quickly dissipated; thus, waters are weakly excited.

To understand how the laser induces conformational changes, Fig. 5 shows the time-evolution of the HBs and secondary structure characteristics of the Aβ peptides. As seen, the fibril does not show any significant structural variations in the absence of the laser. With $E_0 = 2$ V nm^{-1}, C═O bonds are excited and their bond lengths fluctuate around the equilibrium value of 0.123 nm with the maximal amplitude of ≈0.0135 nm [Figs. 3(c) and 4(a)]. As a consequence, intermolecular fibril HBs formed in the fibril structure are broken within the first 5 ps [Fig. 5(a)]. Also, about 80% of the HBs between the C═O amide I atoms and the water molecules (C═O-water) are destroyed [Fig. 5(b)]. After 5 ps, there are no fibril HBs anymore, indicating that the fibril is completely dissociated and converted to a disordered pentamer whose intramolecular HBs then start to reform and increase to a plateau value of ≈12 HBs after 20 ps when the system establishes thermal equilibrium with the solvent molecules [Fig. 5(c)]. The remaining C═O-water HBs (≈20%) will stabilize the nascent monomers and continue to release the excess excitation energy to the heat bath. Interestingly, C═O-water HBs are then reformed and continuously increase up to ≈150 HBs after 50 ps, higher than those formed in the initial fibril structure (≈100 HBs). This is because there are more water molecules around the pentamer than around the fibril. Indeed, we counted the number of water molecules around the Aβ fibril as a function of the cutoff distances between the waters and fibril atoms, and the results shown in Fig. 6 are consistent with the behavior of the C═O-water HBs [Fig. 5(b)].

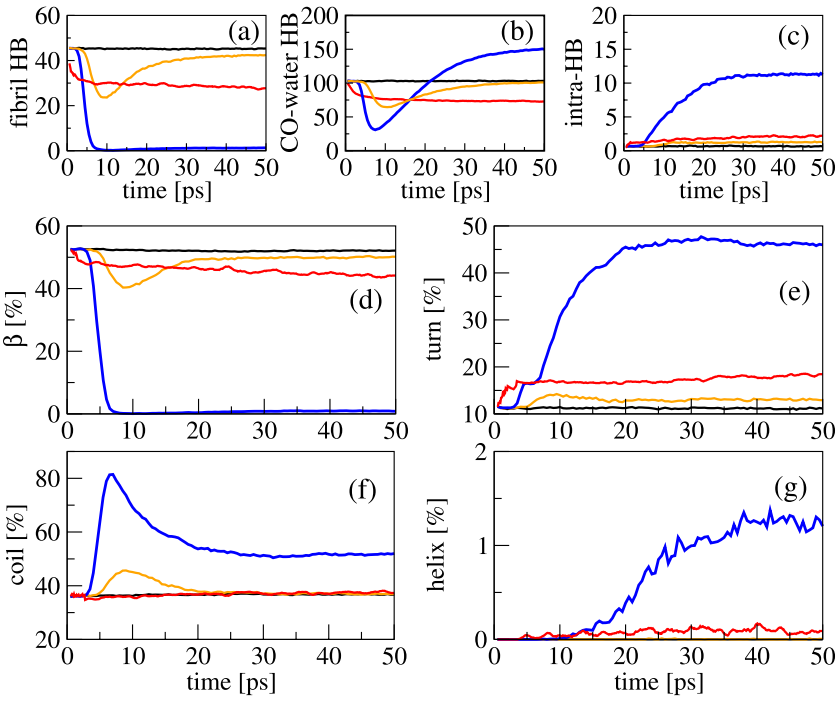

FIG. 5. Time evolution of (a) the intermolecular fibril hydrogen bonds, (b) the C═O amide I atoms and the water molecules hydrogen bonds, (c) the intramolecular hydrogen bonds, and various secondary structure contents (d)–(g). Shown are results of the Aβ in the Aβ-ACP-DNA complex obtained from NEMD simulations using the laser strength $E_0 = 0$ (black), 1 (orange), and 2 (blue) V nm^{-1} and $\omega = 1671$ cm^{-1}. Results of the thermal-induced dissociation simulation (see text for details) are shown in red.

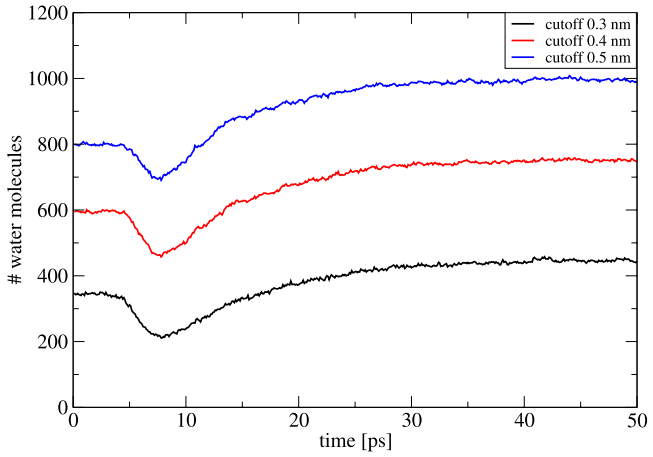

FIG. 6. Time evolution of the number of water molecules around the Aβ fibril in the Aβ-ACP-DNA complex following the excitation with $E_0 = 2$ V nm^{-1}, $\omega = 1671$ cm^{-1}. Shown are results obtained using different cutoff distances between the waters and fibril atoms.

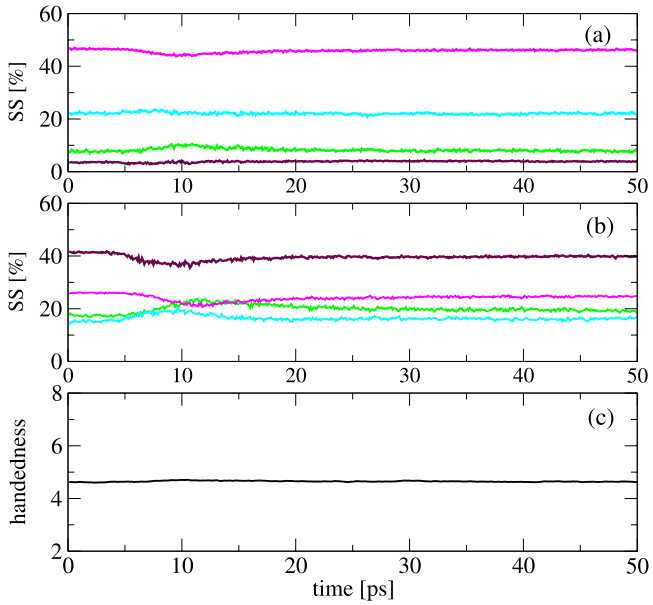

FIG. 7. Time evolution of various secondary structure contents including β (maroon), turn (green), coil (cyan), and helix (magenta) of the PrP protein (a) and ACP protein (b). The result of the handedness of the DNA in the Aβ-ACP-DNA complex is shown in (c). Shown are results obtained using $E_0 = 2$ V nm^{-1}, $\omega = 1671$ cm^{-1}.

Fig. 5 also presents the time evolution of the total population of various secondary structures. During the excitation ($t \leq 10$ ps), the β-structure is almost completely destroyed [Fig. 5(d)], the fibril converts to random coil pentamer as indicated by the significant increase in the coil population from 30% to 80% [Fig. 5(f)], and the turn population increases slightly from its initial 10%-15% value. After excitation ($t \geq 10$ ps), the coil content is quickly reduced as the pentamer starts to fold into turn structure [Fig. 5(e)]. Ultimately, both the turn and coil content end up being approximately equal, and these coexist with a small ($\leq$2%) population of α-helices. Interestingly, after about 20 ps, there are no significant changes in the total secondary structures reflecting that the system is now in a new free energy minimum state. However, the C=O-water HBs still increase indicating that the system is still exploring local free energy minima and that this process proceeds over longer time scales. This indicates the important role played by the waters in the disaggregation process. Importantly, we observed that when using a weaker laser with $E_0 = 1$ V nm^{-1}, the fibril is also destabilized but then quickly refolds back to its initial structure. This suggests that there is a delicate balance between the fibril formation and dissociation. Understanding the factors that are responsible for this balance might provide for important insights into aggregation mechanisms. The laser-induced dissociation mechanism of the Aβ fibril in the Aβ-PrP-DNA complex is quite similar.

D. Effect of laser irradiation on ACP, PrP proteins and DNA

Figs. 7(a) and 7(b) show the time evolution of the secondary structures of the PrP and ACP proteins, respectively. As seen, while the Aβ fibril is completely destroyed [Fig. 5(d)], the PrP is hardly affected [Fig. 7(a)], only very small changes ($\leq$1%) are observed in the secondary structures around 10 ps [Fig. 7(a)]. This is not surprising because the absorption spectrum of the α-rich PrP is red-shifted to 1686 cm^{-1} [Fig. 2(b)]. The ACP is destabilized with larger changes ($\approx$7%) in the secondary structures around 10 ps but then quickly refolds to its initial structure [Figs. 1 and 7(b)]. Because ACP is rich in β structure, its absorption spectrum overlaps with that of the Aβ fibril at $\omega = 1671$ cm^{-1}, but the absorption intensity is much weaker [Fig. 2(c)], thus ACP is less destroyed. Finally, the time-evolution of the handedness reveals that the DNA is also hardly affected by the laser-excitation [Fig. 7(c)].

E. Comparison of laser- and thermal-induced dissociation

Under laser-excitation, the C=O bonds are elongated resulting in the increase of the C=O stretching potential energy. This excess energy is then converted to the kinetic energy and heats locally the C=O atoms [Figs. 4(a) and 4(b)]. It is of interest to compare this laser-induced dissociation with that induced by thermal effect where only kinetic (but no potential) excess energy is included in the C=O bonds. This method has the advantage that the simulation is easier to carry out, but it is clear that a purely kinetic excitation does not represent the correct photo-induced phase-space distribution and may therefore lead to artifacts. To estimate the temperature value for the thermal excitation simulation, we first note that the maximal kinetic energy of a C=O bond received by the laser excitation is about 18 kJ/mol [Fig. 4(b)], which is roughly equivalent to a temperature of 1360 K. Then, we carry equilibrium simulations of the Aβ-ACP-DNA complex where only C=O groups are coupled to the heat bath at 1360 K, and other atoms are maintained at 310 K. As seen from Fig. 4, the fibril is immediately heated, leading to the dissociation, but the conformational changes take place slowly. In contrast, the laser-induced dissociation takes place after 3 ps when the laser intensity starts to increase [Fig. 3(a)], and the fibril is completely dissociated after the laser intensity reaches the maximal value around 6 ps. In the thermal-induced excitation,

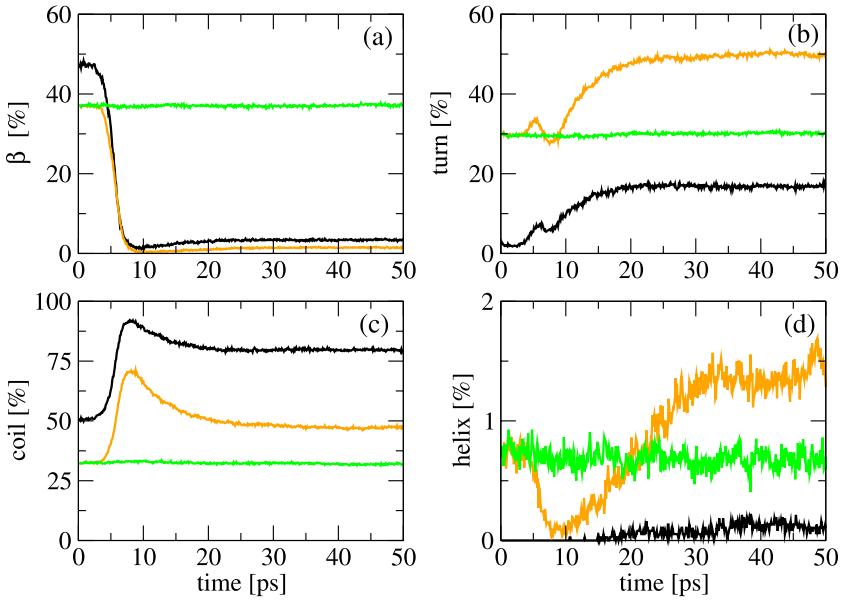

FIG. 8. Time evolution of various secondary structure contents including β (a), turn (b), coil (c), and helix (d). Shown are results obtained using the laser strength $E_0 = 2$ V nm^{-1}, $\omega = 1671$ cm^{-1} for Sup35 (black) and HET-s (orange). The results of HET-s using $E_0 = 2$ V nm^{-1}, $\omega = 1634$ cm^{-1} are shown in green.

velocities of C═O atoms are basically randomly distributed, thus these atoms move randomly, not only along the C═O bond direction but also along other directions. In contrast, the laser deposits energy directly into the C═O bonds via potential energy, and so, the dissociation takes place much faster by targeting directly hydrogen bonds responsible for the structure. This confirms that the laser-induced fibril dissociation process observed in our NEMD simulations is not due to just thermal effects but primarily due to the excitation of the C═O bond stretching vibrations.

F. Laser-induced dissociation of Sup35 and HET-s fibrils

Next, to show that our laser-induced dissociation method is robust and unbiased to fibril structures, we consider the Sup35 and HET-s fibrils whose structures are different from that of the Aβ fibril [Fig. 1]. The time evolutions of various secondary structures of the two systems following the excitation with $E_0 = 2$ V nm^{-1}, $\omega = 1671$ cm^{-1} are displayed in Fig. 8. As seen, the dissociation mechanism is quite similar to that of the Aβ fibril [Fig. 5], where the laser converts primarily the β-structure into random coil oligomers during the excitation ($t \leq 10$ ps) [Figs. 8(a) and 8(c)]. After excitation ($t \geq 10$ ps), the oligomers start to fold into turn structure [Fig. 8(b)]. For the HET-s system, both turn and coil contents end up being approximately equal (≈50%), while the coil population (≈75%) is much higher than the turn content (≈20%) in the Sup35. Both systems display a small (≤2%) α-helical population. For comparison, we also performed a simulation using an off-resonance laser frequency $\omega = 1634$ cm^{-1} and found no significance changes in the structure of the HET-s [Fig. 8]. Snapshots of the configurations as a function of time are shown in Fig. 1.

IV. CONCLUSIONS

We have presented laser-induced NEMD simulations and shown that amyloid fibrils are destroyed due to the strong resonance between the laser field and the amide I vibrational modes of the fibrils. This should be a generic mechanism because of two main reasons. First, most of amyloid fibrils share the same stability characteristics, which is attributed to the highly cooperative nature of the hydrogen bond network throughout the fibrils. Second, the C═O amide I bonds, which participate into that hydrogen bond network, can be excited due to strong resonance with the laser field, leading to the destabilization of the network and subsequently dissociation of the whole fibrils. We demonstrate this with three fibrillar systems having different architectures, and all of them show similar dissociation mechanisms. For the case of Aβ fibril, the irradiation converts the fibril from a deep free energy minimum to a structure containing both turns, coils, and a small population of α-helices. This process is basically finished within 50 ps, but local arrangements between the C═O amide atoms and surrounding water molecules continue over much longer time scales, thereby acting as an efficient cooling channel that prevents the nascent oligomer from overheating. We find that the fibril is destroyed under conditions of high laser power, but that there exists a threshold value at which there is a balance between the fibril formation and dissociation. This reflects the highly resistant property of fibrillar structures. To show the selectivity of laser dissociation, we consider two complexes consisting of the Aβ fibril, surrounded by a DNA and globular proteins ACP and PrP, and we show that the surrounding molecules are hardly affected by the laser excitation. We note that in the reality, a fibril is usually composed of many β-rich chains; thus, its absorption intensity is much stronger than that of globular proteins. Indeed, Hanczyc *et al.* have experimentally shown that amyloids have strong nonlinear optical absorption which is not present in native non-fibrillized proteins.[8] Therefore, the laser is considerably absorbed by the fibril leading to dissociation, while globular proteins have little effects. Furthermore, because the amide I bands of major amyloid fibrils are blue-shifted around 10-20 cm^{-1} compared to globular proteins,[12,40,41] one can target the amide I bands of the fibrils precisely. We should mention that shifts in frequencies of 10-20 cm^{-1} are already large enough in IR

experiments, allowing for an accurate separation between fibrils and globular proteins. Finally, we note that FELs have been applied with some success in human surgery of ablation of biological tissues as well as thermodynamic analyses of biomolecules.[42,43] However, we should remark that adding water periodically to the suspension during irradiation to avoid water evaporation as done in the current experiments[11–14] will be inappropriate if one wants to translate the laser-induced fibril dissociation method into real world applications. This requires further developments.

Taken together, we believe that the laser induced degradation of amyloid fibers can be extremely valuable to further elucidating other structural aspects of fibrils.

ACKNOWLEDGMENTS

P.H.N. thanks Dr. T. Kawasaki for numerous inspiring discussion on the experiments. This work has been supported by the Department of Science and Technology at Ho Chi Minh City, Vietnam (Grant No. 186/HD-SKHCN), the CNRS, IUF, and the National Science Foundation (NSF) USA via Grant No. SI2-1148144. We are grateful to IDRIS for providing computer facilities (Grant No. x2015077198).

[1]O. S. Makinand and L. C. Serpell, FEBS J. **272**, 5950 (2005).
[2]R. Nelsonand and D. Eisenberg, Curr. Opin. Struct. Biol. **16**, 260 (2006).
[3]C. M. Dobson, Nature **418**, 729 (2002).
[4]J. Nasica-Labouze, P. H. Nguyen, O. Berthoumieu, F. Sterpone, N. V. Buchete, S. Cote, A. D. Simone, A. Doig, P. Faller, A. Garcia *et al.*, Chem. Rev. **115**, 3518 (2015).
[5]D. R. Booth, M. Sunde, V. Bellotti, C. V. Robinson, W. L. Hutchinson, P. E. Fraser, P. Hawkins, C. M. Dobson, S. E. Radford, C. C. F. Blake *et al.*, Nature **385**, 787 (1997).
[6]H. Okumuraand and S. G. Itoh, J. Am. Chem. Soc. **136**, 10549 (2014).
[7]G. Leinengaand and J. Gotz, Sci. Transl. Med. **7**, 278ra33 (2015).
[8]P. Hanczyc, M. Samoc, and B. Norden, Nat. Photonics **7**, 969 (2013).
[9]D. Ozawa, H. Yagi, T. Ban, A. Kameda, T. Kawakami, H. Naiki, and Y. Goto, J. Biol. Chem. **284**, 1009 (2009).
[10]H. Yagi, D. Ozawa, K. Sakurai, T. Kawakami, H. Kuyama, O. Nishimura, T. Shimanouchi, R. Kuboi, H. Naiki, and Y. Goto, J. Biol. Chem. **285**, 19660 (2010).
[11]T. Kawasaki, J. Fujioka, T. Imai, and K. Tsukiyama, Protein J. **31**, 710 (2012).
[12]T. Kawasaki, J. Fujioka, T. Imai, K. Torigoe, and K. Tsukiyama, Lasers Med. Sci. **29**, 1701 (2014).
[13]T. Kawasaki, T. Imai, and K. Tsukiyama, J. Anal. Sci., Methods Instrum. **4**, 9 (2014).
[14]T. Kawasaki, T. Yaji, T. Imai, T. Ohta, and K. Tsukiyama, Am. J. Anal. Chem. **5**, 384 (2014).
[15]T. Lührs, C. Ritter, M. Adrian, D. Riek-Loher, B. Bohrmann, H. Döbeli, D. Schubert, and R. Riek, Proc. Natl. Acad. Sci. U. S. A. **102**, 17342 (2005).
[16]J. Lauren, D. A. Gimbel, H. B. Nygaard, J. W. Gilbert, and S. M. Strittmatter, Nature **457**, 1128 (2009).
[17]M. Thunnissen, N. Taddei, G. Liguri, G. Ramponi, and P. Nordlund, Structure **5**, 69 (1997).
[18]R. Nelson, M. R. Sawaya, M. Balbirnie, A. Madsen, C. Riekel, R. Grothe, and D. Eisenberg, Nature **435**, 773 (2005).
[19]C. Wasmer, A. Lange, H. van Melckbeke, A. B. Siemer, R. Riek, and B. H. Meier, Science **319**, 1523 (2008).
[20]M. Moradi, V. Babin, C. Roland, and C. Sagui, Nucleic Acids Res. **41**, 33 (2012).
[21]K. Lindorff-Larsen, S. Piana, K. Palmo, P. Maragakis, J. L. Klepeis, R. O. Dror, and D. Shaw, Proteins: Struct., Funct., Bioinf. **78**, 1950 (2010).
[22]E. Lindahl, B. Hess, and D. van der Spoel, J. Mol. Mod. **7**, 306 (2001).
[23]J. P. Ryckaert, G. Cicotti, and H. J. C. Berendsen, J. Comput. Phys. **23**, 327 (1977).
[24]T. Darden, D. York, and L. Pedersen, J. Chem. Phys. **98**, 10089 (1993).
[25]H. J. C. Berendsen, J. P. M. Postma, W. F. van Gunsteren, A. Dinola, and J. R. Haak, J. Chem. Phys. **81**, 3684 (1984).
[26]C. Calemanand and D. van der Spoel, Angew. Chem., Int. Ed. **47**, 1341 (2008).
[27]D. van der Spoel, F. R. N. C. Maia, and C. Caleman, Phys. Chem. Chem. Phys. **42**, 6344 (2008).
[28]V. Botan, E. H. G. Backus, R. Pfister, A. Moretto, M. Crisma, C. Toniolo, P. H. Nguyen, G. Stock, and P. Hamm, Proc. Natl. Acad. Sci. U. S. A. **104**, 12749 (2007).
[29]P. H. Nguyen and G. Stock, Chem. Phys. **323**, 36 (2006).
[30]P. H. Nguyen, R. D. Gorbunov, and G. Stock, Biophys. J. **91**, 1224 (2006).
[31]E. H. G. Backus, P. H. Nguyen, V. Botan, R. Pfister, A. Moretto, M. Crisma, C. Toniolo, G. Stock, and P. Hamm, J. Phys. Chem. B **112**, 9091 (2008).
[32]S. Y. Park, P. H. Nguyen, and G. Stock, J. Chem. Phys. **131**, 184503 (2009).
[33]P. H. Nguyen, S. Y. Park, and G. Stock, J. Chem. Phys. **132**, 025102 (2010).
[34]D. Frishmanand and P. Argos, Proteins **23**, 566 (1995).
[35]E. B. Wilson, J. C. Decius, and P. C. Cross, *Molecular Vibrations* (Dover Publications, New York, 1980).
[36]A. D. MacKerell, Jr., D. Bashford, M. Bellott, R. L. Dunbrack, J. D. Evanseck, M. J. Field, S. Fischer, J. Gao, H. Guo, S. Ha *et al.*, J. Phys. Chem. B **102**, 3586 (1998).
[37]G. A. Kaminski, R. A. Friesner, J. Tirado-Rives, and W. L. Jorgensen, J. Phys. Chem. B **105**, 6474 (2001).
[38]W. van Gunsteren, S. R. Billeter, A. A. Eising, P. H. Hünenberger, P. Krüger, A. E. Mark, W. Scott, and I. Tironi, *Biomolecular Simulation: The GROMOS96 Manual and User Guide* (Vdf Hochschulverlag AG an der ETH, Zurich, 1996).
[39]Y. Wu, H. L. Tepper, and G. A. Voth, J. Chem. Phys. **124**, 024503 (2006).
[40]H. L. Zhu, S. R. Meng, J. B. Fan, J. Chen, and Y. Liang, PLoS One **6**, e25020 (2011).
[41]M. Jackson and H. H. Mantsch, Can. J. Chem. **69**, 1639 (1991).
[42]M. A. Mackanos, D. Simanovskii, K. M. Joos, H. A. Schwettman, and E. D. Jansen, Lasers Surg. Med. **39**, 230 (2007).
[43]G. Edwards, Laser Photonics Rev. **3**, 545 (2009).